Journal of Metals, Materials and Minerals, 36(2), e2518, 2026

An integrated experimental–numerical approach for characterizing deformation behavior of high-strength steels

Weerapong JULSRI[1], Apichat SANRUTSADAKORN[1], and Vitoon UTHAISANGSUK[2,*]

[1] *Department of Industrial Engineering, Faculty of Industry and Technology, Rajamangala University of Technology Isan (RMUTI), Sakon Nakhon Campus, Sakon Nakhon 47160, Thailand*

[2] *Center for Lightweight Materials, Design, and Manufacturing, Department of Mechanical Engineering, Faculty of Engineering, King Mongkut's University of Technology Thonburi (KMUTT), Bangmod, Bangkok 10140, Thailand*

***Corresponding author e-mail**: vitoon.uth@kmutt.ac.th

Received date:
27 September 2025
Revised date:
13 November 2025
Accepted date:
17 November 2025

Keywords:
Nakajima tests;
Forming limit curves (FLCs);
Forming limit stress curves (FLSCs);
High-strength steel;
Hardening model

Abstract

This study aims to establish an integrated experimental–numerical framework for characterizing the deformation behavior of DP590 high-strength steel sheet. The framework combines experimental uniaxial tensile and Nakajima tests with finite element (FE) simulations to provide a comprehensive assessment of forming limits and fracture behavior. Forming limit curves (FLCs) and forming limit stress curves (FLSCs) were determined with the integrated approach and then validated numerically using the Hill'48 yield criterion together with both Swift and Voce hardening laws. Model calibration incorporated experimental data on directional mechanical properties to ensure that material anisotropy was accurately represented. The FE simulations demonstrated strong agreement with the experimental data across uniaxial, plane-strain, and biaxial loading paths. The Swift hardening law consistently predicted higher forming limit stresses and more accurate drawing-depth estimates than the Voce law, particularly under biaxial and plane-strain conditions. The novelty of this work lies in the simultaneous validation of both strain- and stress-based forming limits, combined with the quantitative prediction of drawing depths, which has rarely been reported for DP590 grade. The proposed framework improves the predictive accuracy of forming simulations and provides practical guidelines for material characterization and process optimization in the automotive and related manufacturing industries.

1. Introduction

The automotive industry is increasingly focusing on optimizing vehicle materials to meet regulatory standards, competitive demands, consumer preferences, and financial challenges. To achieve these objectives, manufacturers strive to reduce material costs while improving manufacturability, collision energy absorption, and fuel efficiency, as well as lowering greenhouse gas emissions throughout the vehicle's lifecycle. High-strength steel (HSS) plays a pivotal role in these efforts, as its high strength-to-weight ratio enables the production of lighter and more durable components that enhance fuel efficiency and reduce emissions, aligning with both environmental and economic goals [1,2]. However, the forming of HSS presents significant challenges due to its limited ductility, which increases the risk of cracking and makes the forming of complex geometries more difficult. Additionally, its anisotropic properties further complicate stress prediction, necessitating the use of advanced tools such as Forming Limit Curves (FLCs) and Forming Limit Stress Curves (FLSCs) to ensure reliable forming processes and efficient material utilization [3,4]. These tools allow engineers to optimize forming processes, reduce defects, improve material usage, and minimize waste—factors that are essential for efficient and sustainable manufacturing.

Forming limit curves (FLCs) and forming limit diagrams (FLDs) are strain-based criteria typically used to describe the onset of localized necking. In contrast, forming limit stress curves (FLSCs) and forming limit stress diagrams (FLSDs) are stress-based criteria that provide a path-independent description of forming limits and are less sensitive to strain history. Although FLC/FLD approaches are widely used in industry, the FLSC/FLSD approach offers notable advantages for simulations involving complex, nonlinear loading paths. In this study, both approaches are compared to provide a more comprehensive evaluation of formability of HSS. Integrating strain- and stress-based forming limits with experimental testing and numerical simulations further enhances the accuracy of sheet-metal formability assessment. Common testing methods, such as the Nakajima and Marciniak tests, are widely used to determine strain limits by examining necking or failure points under controlled deformation conditions, which is essential for precise formability evaluation [3,4].

In parallel, studies on dual-phase steels have employed FE simulations of two-dimensional representative volume elements (RVEs) generated from real micrograph analyses to model material behavior under various loading conditions. The flow behavior of individual phases in DP steels has been described using dislocation theory and local chemical composition. Predicted stress–strain responses have been

mostly validated against experimental tensile data. This multiscale approach enables more realistic simulation of material behavior under actual forming conditions, thereby improving the predictive capability of FLCs and FLSCs for dual-phase steels [5]. Moreover, research on advanced high-strength steels (AHSS) has implemented FEA-based simulations that incorporate anisotropy and strain-rate sensitivity to better capture material behavior under different loading paths, ultimately improving the accuracy of failure predictions in complex forming scenario.

Finite element analysis (FEA) has been widely used to predict forming limit curves (FLCs) by simulating material behavior under varying loading conditions and incorporating properties such as anisotropy, strain-rate sensitivity, and hardening to accurately model failure mechanisms [7]. FEA has also been applied with forming limit diagrams (FLDs) and forming limit stress diagrams (FLSDs) to evaluate both stress and strain developments of sheet metal under uniaxial and biaxial deformations, enabling more precise failure predictions [8]. In automotive applications, FEA has been extensively used to analyze AHSS grades 780, 980, and 1180, focusing on mechanical behavior, formability, and crash performance. Through combined experimental testing and simulation, FLCs and FLSCs have been established, allowing engineers to evaluate key properties such as formability, springback, and crashworthiness, thereby supporting design and manufacturing decisions [9]. The influence of nonlinear strain paths on FLDs has also been investigated using the Marciniak–Kuczynski (M–K) model with both isotropic and anisotropic hardening laws. These studies have shown that loading paths significantly influence material formability [10]. Nonlinear strain-path effects observed in Nakajima tests further highlight the need for advanced constitutive models to improve prediction accuracy [11]. Accurate material modeling is essential for assessing formability and predicting failure using FLCs and FLSCs under diverse forming conditions. Models such as the Marciniak–Kuczynski (M–K), Hill'48, Barlat89, and Barlat2000, together with hardening laws such as Swift and Voce, have been widely used to predict localized necking in sheet metals, providing valuable information for determining FLCs and FLSCs [12–17].

The establishment of a constitutive model for high-strength steels (HSS) requires a comprehensive evaluation of material properties as well as the associated computational complexity. Previous studies have summarized the key considerations for constructing HSS constitutive models and analyzed their application in practical research and development [18]. Extensive research has also focused on developing and refining forming limit curves (FLCs) and forming limit stress curves (FLSCs) for high-strength steels. For example, Panich *et al.* (2017) experimentally developed strain-based fracture forming limit curves for advanced high-strength steel grade 980 using Nakajima stretch-forming tests and tensile tests under shear deformation [3]. Similarly, Huang and Shi (2018) employed experimental and empirical approaches to predict FLCs for high-strength steels [6]. Panich *et al.* (2021) demonstrated that analyses based on FLCs and FLSCs enhance forming accuracy, reduce defects, improve product quality, and optimize manufacturing processes for high-strength steel applications [19]. Bornancin *et al.* (2023) further confirmed the importance of FLC and FLSC studies in improving forming-process precision, reducing defects, and optimizing industrial production techniques [7]. More recent developments include the work of Béres *et al.* (2023), who introduced a novel forming limit diagram that highlights wrinkling behavior and the influence of normal pressure on clamped surfaces. Their study employed finite element modeling to assess wrinkling in steel sheets under compressive and circumferential stresses [20]. Zhang *et al.* (2024) proposed a dual-stage forming limit curve method for fiber metal laminates (FMLs), effectively preventing wrinkling and delamination and improving progressive damage predictions under complex strain paths [21]. Zhang *et al.* (2024) developed a comprehensive forming-limit framework incorporating localization, ductile fracture, and cleavage fracture mechanisms in AHSS, demonstrating how these failure modes interact under different stress states to improve formability predictions in complex loading scenarios [22]. In addition, Tao Huang *et al. (*2019) applied the GTN model to predict the forming limit stress diagram (FLSD) of TA1 titanium sheets. Using finite element inverse calibration and hemispherical punch stretching tests, the study established GTN parameters for accurate FLSD prediction [23]. Hongjian Cui *et al.* (2023) investigated FLSD development for high-strength dual-phase steels using stress-based fracture criteria, with Nakajima test data and FE simulations confirming improved accuracy in formability prediction under complex strain states [24]. Overall, research on FLCs and FLSCs provides significant industrial benefits by enabling precise determination of forming limits, reducing defects, improving product quality, and enhancing production efficiency. These tools also minimize material waste and support the development of new materials and forming technologies—benefits that are particularly valuable to the automotive and aerospace sectors.

Although the FLCs and FLSCs have been widely investigated for high-strength steels, most previous studies have focused on higher grades such as DP780 or DP980 and have often relied exclusively on strain-based criteria or a single hardening law. Systematic investigations that combine both strain-based and stress-based forming limits with FE simulations for DP590 grade remain scarce, despite its increasing use as a thin-gauge structural material in the automotive sector.

To address this gap, the present study establishes an integrated experimental–numerical framework for characterizing the deformation behavior of DP590 grade high-strength steel. Uniaxial tensile tests and Nakajima experiments were performed to determine forming limits, which were subsequently validated using FE simulations based on the Hill'48 yield criterion. Two representative hardening laws—Swift and Voce—were systematically compared. The novelty of this work lies in the simultaneous validation of strain- and stress-based forming limits across uniaxial, plane-strain, and biaxial loading paths, together with the quantitative evaluation of drawing-depth predictions of formed samples. This comprehensive approach provides new insights into the role of anisotropy and hardening behavior in the formability of DP590 steel and offers practical guidelines for selecting constitutive models to enhance the predictive accuracy of industrial forming simulations.

2. Materials models

2.1 Hill'48 yield criterion.

The Hill'48 anisotropic yield criterion [13] is formulated using a quadratic function to describe the yield behavior along the principal material axes, which typically correspond to the rolling, transverse,

and normal directions of a sheet metal sample. This criterion provides a framework for assessing material anisotropy in metal-forming processes by incorporating directional dependencies in the yield stress, as shown in Equation (1).

$$\bar{\sigma}_{\text{Hill}} = \sqrt{F\sigma_{xx}^2 + G\sigma_{xx}^2 + H(\sigma_{xx} - \sigma_{yy})^2 + 2N\sigma_{xy}^2} \quad [1]$$

where F, G, H, and N are the parameters representing the current state of anisotropic yielding behavior of material, σ_{xx} and σ_{yy} are the principal stresses ($\sigma_{xx} = \sigma_1$ and $\sigma_{yy} = \sigma_2$), and σ_{xy} is the shear stress component considered in the analysis. As reported by Stoughton [25], these material parameters of the Hill'48 function can be expressed in terms of the tensile and shear yield stresses associated with the principal anisotropic directions. Therefore, the relationships between the strain ratio (α) and stress ratio (ρ), as well as the stress ratio parameter considering anisotropic characteristics, were derived from the Hill'48 yield function, as shown in Equation (2) and Equation (3), respectively.

$$\rho_{\text{Hill}} = \frac{(F+H)\cdot\alpha - H}{G+H-H\alpha} \quad [2]$$

$$\xi_{\text{Hill}} = \frac{\sigma_{\text{Hill}}}{\sigma_1}\sqrt{(G+H) + (F+H)\alpha^2 - 2H\alpha} \quad [3]$$

The Hill'48 yield criterion is widely used to describe anisotropic yielding behavior in sheet metals. Its material parameters are determined from experimental data and are strongly influenced by the plastic anisotropy of the material.

The r-values, also known as the Lankford coefficient, is defined as the ratio of true width strain to true thickness strain, as given in Equation (4), which can be obtained from uniaxial tensile tests.

$$r = \frac{\varepsilon_w}{\varepsilon_t} \quad [4]$$

obtained from uniaxial tensile tests. In this study, r-values were measured in three directions relative to the rolling direction of the sheet metal: r_0 (parallel to rolling direction, RD), r_{45} (diagonal direction, DD), and r_{90} (transverse direction, TD). These r-values characterize the material's anisotropy and are essential for understanding its directional yield behavior.

The relationships between these r-values and Hill's parameters (F, G, H, and N) were derived using the associative flow rule, as given in Equation (5). This calibration ensures that the yield function correctly represents the directional dependence of plastic deformation for DP590 steel.

$$F = \frac{r_0}{r_{90}(1+r_0)},\ G = \frac{1}{1+r_0},\ H = \frac{r_0}{1+r_0},\ \text{and } N = \frac{(r_0 + r_{90})\cdot(1+2r_{45})}{2r_{90}\cdot(1+r_0)} \quad [5]$$

2.2 Hardening laws

2.2.1 Swift hardening law

The flow curve obtained from the tensile test was fitted using the Swift hardening law [16], as shown in Figure 2, and compared with the results from the tensile test in the RD direction. The material's flow behavior during plastic deformation is mathematically described by the Swift hardening model, as given in Equation (6).

$$\bar{\sigma} = K(\bar{\varepsilon}_0 + \bar{\varepsilon}_p)^n \quad [6]$$

Here, $\bar{\sigma}$ and $\bar{\varepsilon}_p$ represent the equivalent stress and equivalent plastic strain, respectively. The other three parameters, K, n, and $\bar{\varepsilon}_0$, denote the strength coefficient, strain hardening exponent, and equivalent elastic strain, respectively. All material constants were determined through the curve-fitting process. The flow curve obtained from the sheet deformation under uniaxial tension in the RD direction, as shown in Figure 2, was used to describe the strain hardening behavior of the studied DP590 steel.

2.2.2 Voce hardening law

The Voce hardening law [17] is a constitutive model used to describe the hardening behavior of materials, particularly metals, during plastic deformation. The Voce law captures the gradual saturation of stress as the material deforms plastically. This is particularly important for materials that do not exhibit a simple linear hardening behavior. The model provides a smooth transition from the initial yield stress to the saturation stress, making it useful for modeling continuous hardening processes, as given in Equation (7).

$$\sigma(\varepsilon_p) = \sigma_0 + (\sigma_s - \sigma_0)\left[1 - \exp(-k\varepsilon_p)\right] \quad [7]$$

σ is the stress as a function of plastic strain ε_p. σ_0 is the initial yield stress. σ_s is the saturation stress, representing the maximum stress achievable at large strains. k is the material constant that controls the rate at which the stress approaches the saturation stress. ε_p is the plastic strain.

3. Materials characterization

3.1 Tensile test and anisotropic parameters

Uniaxial tensile tests were performed to determine the anisotropic plastic behavior of DP590 steel sheets with a thickness of 1 mm. The specimens were prepared in accordance with DIN EN 10002-1 standards using a gauge length of 50 mm and tested at a constant crosshead speed of 0.01 mm·s^{-1}, corresponding to an engineering strain rate of approximately 0.0002 s^{-1}. To evaluate directional dependence, the specimens were cut and tested in three orientations: rolling direction (RD), diagonal direction (DD), and transverse direction (TD). Figure 1 presents the true stress–strain curves obtained from the three orientations, demonstrating anisotropic mechanical responses. The RD specimens had the highest yield strength, ultimate tensile strength, and elongation of all the directions tested. This means that they were better able to resist deformation along the rolling direction. Mechanical properties, including elastic modulus (E), 0.2% offset yield strength (YS), ultimate tensile strength (UTS), uniform elongation, total elongation, and plastic strain ratio (r-values), were calculated from three repeated tests in each direction. These results, reported as mean ± standard deviation (SD), are summarized in Table 1.

Table 1. Tensile properties of high-strength steel sheets of DP590 grade.

Direction	*E* [GPa]	*YS* (0.2% offset) [MPa]	*UTS* [MPa]	% Elongation Uniform	*E* Total	*r*-value
RD-1	154.31	466.83	634.28	13.98	26.13	1.01
RD-2	152.27	464.28	628.45	14.19	25.11	0.99
RD-3	151.72	455.72	631.36	14.07	24.01	0.96
Mean ± SD	152.10 ± 1.29	462.28 ± 5.84	631.36 ± 2.90	14.08 ± 0.11	25.08 ± 0.86	0.99 ± 0.02
DD-1	155.35	454.92	632.15	14.5	24.27	1.14
DD -2	150.51	437.72	626.86	13.04	23.91	1.14
DD -3	152.77	447.82	630.56	14.54	23.77	1.12
Mean ± SD	152.88 ± 2.42	446.82 ± 8.67	629.86 ± 2.82	14.03 ± 0.86	23.98 ± 0.26	1.13 ± 0.01
TD-1	158.82	417.17	633.88	13.79	23.98	0.9
TD -2	164.62	411.51	627.48	13.94	24.03	0.89
TD -3	161.7	411.34	628.55	13.93	24.05	0.94
Mean ± SD	161.71 ± 2.90	413.34 ± 3.33	629.97 ± 3.48	13.93 ± 0.07	24.02 ± 0.03	0.91 ± 0.03

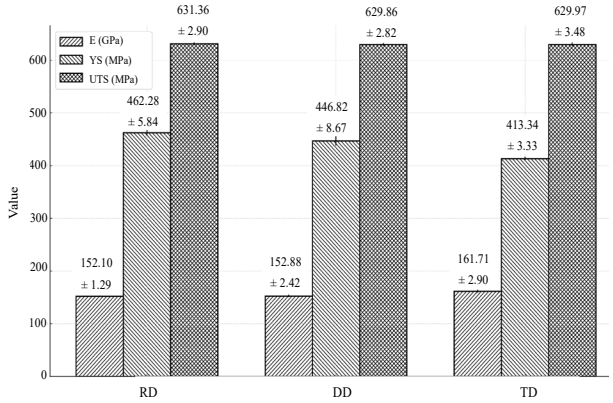

Figure 1. Tensile properties (*E*, *YS*, *UTS*) of the high-strength steel sheet of DP590 grade, presented as mean ± standard deviation for the RD, DD, and TD directions.

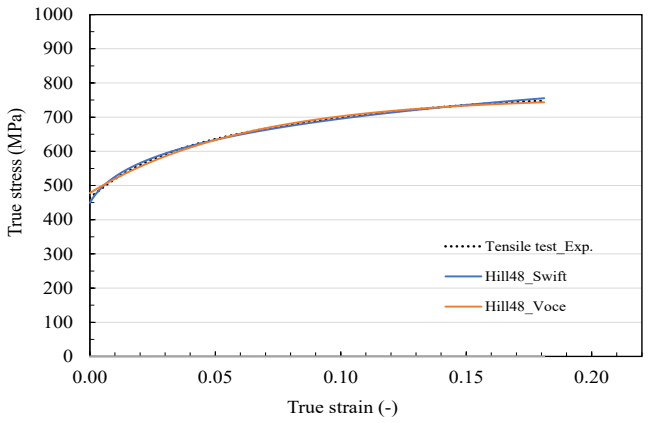

Figure 2. Flow stress curves obtained experimentally from tensile tests and extrapolated using the Swift and Voce hardening laws.

To determine the anisotropic material parameters in the Hill'48 yield criterion, yield stresses and *r*-values obtained from various loading conditions were used. These parameters provide essential insights into the material's directional behavior under stress, enabling accurate modeling of anisotropy. Specifically, in the Hill'48 model, all parameters were determined using Equation (1), based on the *r*-values derived from tensile tests conducted in various orientations relative to the sheet's rolling direction. These *r*-values reflect the material's resistance to thinning and its ability to undergo plastic deformation in different directions. Table 2 presents the calculated anisotropic coefficients of the Hill'48 function for the examined HSS sheet, indicating how the material's yield stresses vary along different axes. These coefficients enable precise modeling of anisotropic yielding, essential for applications that require accurate predictions of material behavior under complex loading conditions. By incorporating both the yield stresses and r-values, the Hill'48 model provides a more detailed and reliable representation of the HSS sheet' s anisotropic characteristics, thereby enhancing the accuracy of formability analyses and structural simulations. In this study, the flow curve obtained from uniaxial tension tests in the RD, as shown in Figure 2, was used to characterize the strain hardening behavior of the investigated steel. This curve serves as the basis for understanding how the material hardens under strain, with further details provided in Table 3-4.

3.2 Nakajima forming tests

In the Erichsen test setup, a 100 mm diameter semi-circular dome-shaped punch, as illustrated in Figure 3, was utilized to analyze the metal forming process. As shown in Figure 4, the setup employed a lock bed to control and halt the flow of metal, ensuring a precise forming process. The punch applied a maximum force of 400 kN, representing a high-stress condition suitable for testing the material's formability. Additionally, a blank holder with a maximum force of 200 kN was employed to secure the metal sheet in place, minimizing any movement that could interfere with the forming process. This combination of forces created a controlled environment to observe the material's behavior as it formed into a semi-circular dome, as illustrated in Figure 5.

Table 2. Anisotropic coefficients of the Hill'48 model based on the *r*-values for the investigated high-strength steel.

F	*G*	*H*	*N*
0.55	0.50	0.50	1.71

Table 3. Material constants of the Swift hardening.

K	ε_0	*n*
963.46	0.01	0.15

Table 4. Material constants of the Voce hardening.

σ_0	σ_s	k
478.18	280.86	16.05

Table 5. Dimensions of the specimens used in Nakajima tests.

Nakajima specimen	Samples No.	W [mm]
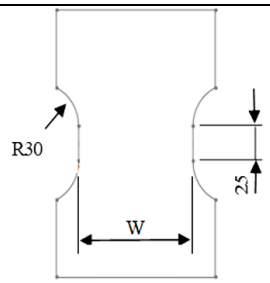	1	20
	2	50
	3	80
	4	90
	5	100
	6	130
	7	140
	8	160
	9	190

Figure 3. Erichsen testing machine.

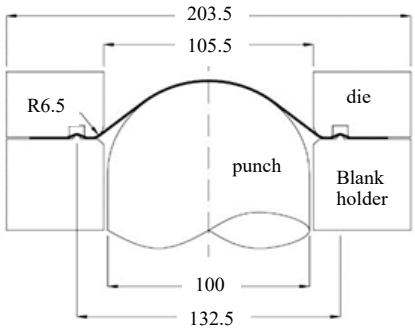

Figure 4. Dimensions and setup of the semi-circular dome used in the Erichsen test.

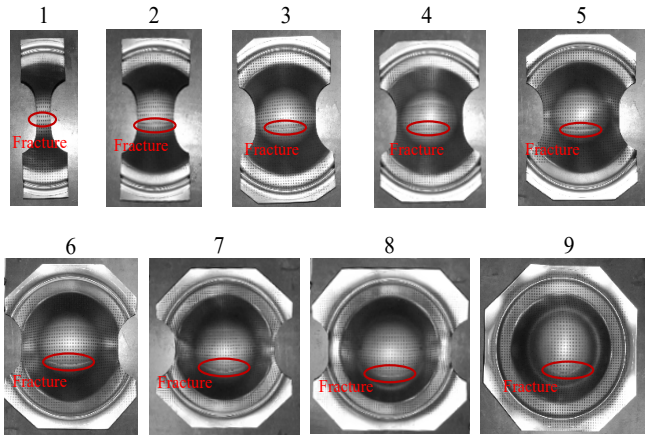

Figure 5. Fractured samples after the Nakajima tests.

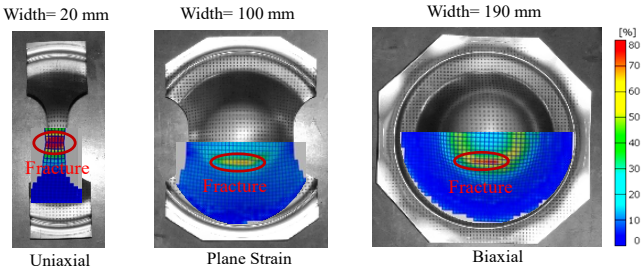

Figure 6. Major engineering strains measured by DIC at the fracture states.

The Nakajima tests were conducted using a 100 mm diameter dome, in accordance with the standard Nakajima test procedure. The dimensions of the samples used in the tests, prepared following the ASTM E 2218-02 standard, are depicted in Table 5. Each of the nine sheet specimens had a length of 190 mm, with widths ranging from 20 mm to 190 mm, resulting in nine different strain paths on each specimen. To detect surface strain, the entire surface of each blank was uniformly electrochemically etched with a 3-mm grid.

The tests were carried out under a constant blank holder force and a forming speed of 10 mm·min^{-1} until fracture occurred. To minimize friction between tool and sheet metal, SAE40 lubricant oil was applied consistently prior to each test. Occasional off-center fractures were attributed to minor local variations in lubrication distribution, which did not significantly affect the repeatability of the forming limit measurements. All specimens reached fracture after the punch formed a dome with a 100 mm diameter, marking the onset of failure for each case. These samples formed part of the Nakajima test series, designed to evaluate formability limits under stretching conditions.

Figure 5 presents the experimental fracture patterns observed in the Nakajima tests under different strain paths. Under uniaxial tension, the specimens exhibited a typical cup-and-cone fracture morphology, indicating localized necking followed by ductile shear failure. In plane strain conditions, fractures were predominantly defined by pronounced shear bands and minimal thinning, indicating the material's constrained ability to redistribute strain. In biaxial loading, diffuse necking and equiaxial thinning were observed prior to fracture, which is consistent with stress triaxiality-driven damage mechanisms. These observations highlight the influence of loading paths on failure behavior and provide essential physical evidence supporting the experimentally determined forming limit curves (FLCs) and forming limit stress curves (FLSCs). The local strain distributions on the deformed samples were then measured using a digital image correlation (DIC) strain measurement system. The DIC system measured the major and minor engineering strains at the fracture state, as shown in Figure 6 [4,8,26]. Based on these results, the achievable strains at the onset of fracture for each specimen were identified, with the fracture and necking zones near the crack path distinguished.

4. Determination of FLCs and FLSCs

The fractured specimens after stretching are displayed in Figure 5, which illustrates the formation process of necks and cracks. In these tests, a deformed grid circle was applied, carefully designed to account for material strains. This grid provides a visual reference for analyzing the material's strain distribution during deformation [4,8,26]. During analysis, it is essential to select deformed grid areas that are unaffected

by cracks, ensuring accurate strain measurements without interference from fracture patterns. Testing of high-strength steel sheets grade 590 revealed that cracks predominantly formed near the top of the dome, suggesting a concentration of strain in this area under applied stress. Strain measurements were taken at points of localized necking and fracture to develop FLCs. Specifically, nine localized necking strain values from different specimens were recorded to represent critical strain levels that indicate the material's limits before failure. In these Nakajima tests, strain data were obtained by measuring the major and minor strains, enabling precise plotting of the forming limit curve. Figure 7(a) displays the resulting FLCs, which outline the deformation limits of high-strength steel sheets and provide a critical reference for the forming behavior of grade 590 steel under stretch conditions. This information is crucial for optimizing forming processes, as it highlights the material's threshold for ductility and resistance to fracture, aiding in the prevention of material failure in practical applications.

FE simulations were conducted in Dynaform software to replicate the sheet metal forming process. The experimental forming setup utilized a 100 mm diameter hemispherical punch. The die, punch, and binder, as shown in Figure 4, and the blank sample (as described in Table 5), along with the boundary conditions, were defined in the simulations to match the experimental setup. The blank was meshed using shell elements, while all other components were modeled as rigid bodies. The square shell element with a size of 2 mm × 2 mm was defined. The type 2 (Belytschko-Tsay) element formulation with a single integration point through the thickness was adopted. Additionally, the anisotropic material models, namely Hill'48, using both the Swift and Voce hardening laws was applied along with the different obtained parameter sets in Tables 1–4. A friction coefficient of $\mu = 0.125$ was selected based on calibration with experimental dome heights, ensuring consistency between experimental and numerical forming behavior. The punch velocity was set to 10 mm·min^{-1}.

From FE results of Nakajima forming tests, the critical major and minor stress values at the fracture states of each sample were gathered to plot the FLSCs, are presented in Figure 7(b). These simulations utilized the Hill'48 yield criterion along with both the Swift and Voce hardening models [13,16,17]. The analysis revealed that the Swift hardening model yielded slightly higher FLSCs compared to the Voce hardening model. This difference is due to the distinct hardening behaviors of the two models. The Swift hardening model predicts a more rapid increase in material strength during deformation, resulting in a higher stress-bearing capacity. In contrast, Voce hardening describes a more gradual increase in strength, leading to lower forming limit stresses under similar conditions. The selection of a hardening model significantly influences metal forming analysis, as it affects the predictions of the material's stress tolerance and strain limits during processing.

5. Verification

Figure 8 shows the verification of the determined FLC for the high-strength steel sheets grade DP590 by comparing experimental results regarding strain paths obtained from the Nakajima tests. The strain path plots of major and minor strains, representing various loading modes, including uniaxial, plane strain, and biaxial regions. The resulting strain paths showed the material's responses under different stress state conditions. The color scale indicates equivalent strain values, highlighting areas of higher strain concentrations, particularly under the biaxial condition. The verification results indicated that the Swift hardening consistently predicted higher forming limit stresses than the Voce model, especially under the plane strain and biaxial states [29,30]. This comparison shows that the models predicted different material behaviors under the examined forming conditions.

The differences observed between the Swift and Voce hardening models can be physically interpreted in terms of strain hardening behavior and anisotropy effects. The Swift model, with its continuously increasing strain hardening capacity, tends to delay the onset of localized necking, thereby predicting higher forming limits and drawing depths, particularly under plane strain and biaxial loading. The Voce model, on the other hand, saturates more quickly, which means that strain hardening is limited and formation limit predictions are lower. This explains why the deviations between the two models become more pronounced in multiaxial stress states, where the ability to accommodate additional strain before instability is crucial. Furthermore, experimental observations confirm that the anisotropy of DP590, as characterized by the *r*-values, strongly influences strain localization patterns. Higher *r*-values in certain directions enhance resistance to thinning, whereas lower *r*-values promote earlier localization, consistent with the differences captured in the FE simulations. These findings provide a mechanistic link between the constitutive description of hardening and the experimentally observed fracture behavior, thereby reinforcing the validity of the integrated experimental–numerical approach.

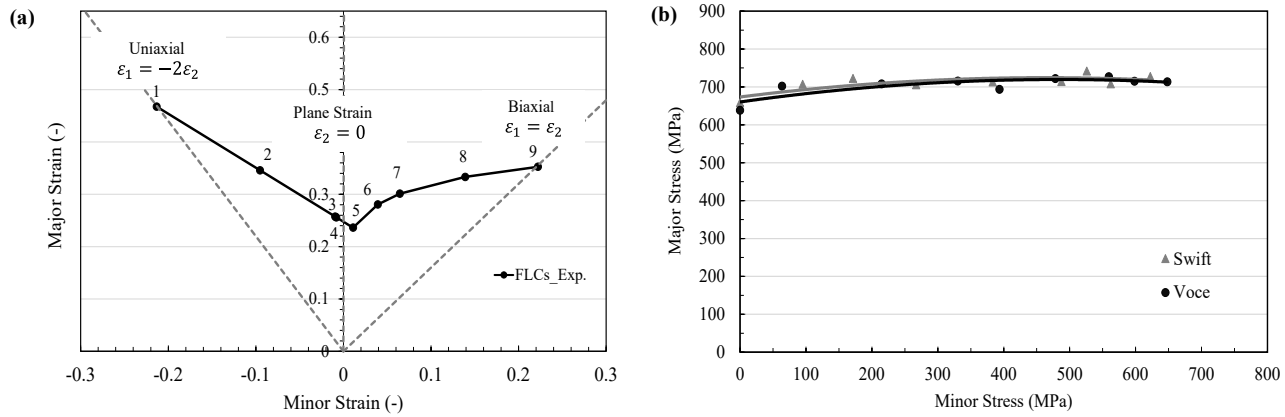

Figure 7. Determined (a) FLC, and (b) FLSCs of the investigated steel.

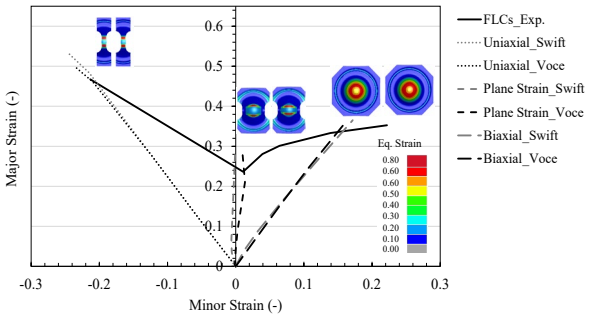

Figure 8. Verification of the determined FLC of high-strength steel sheets grade DP590 using various strain paths obtained from the Nakajima tests.

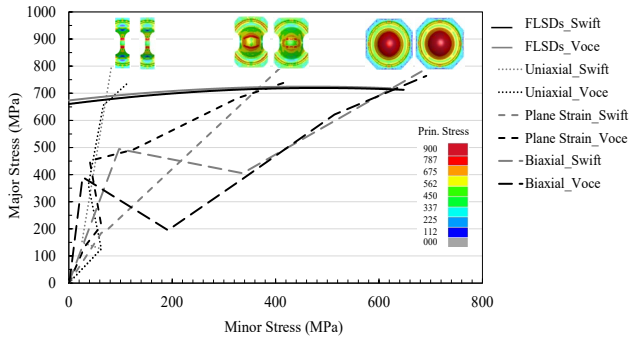

Figure 9. Verification of the determined FLSCs of high-strength steel sheets grade DP590 using various stress paths obtained from the Nakajima tests.

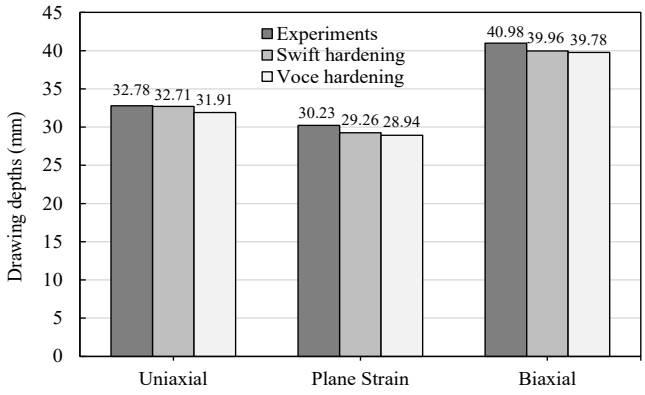

Figure 10. Comparison between experimentally determined and predicted drawing depths under uniaxial, plane strain, and biaxial samples at fracture for the investigated high-strength steel.

Figure 9 illustrates the verification of the determined FLSCs for the high-strength steel sheets of DP590 grade, comparing them with stress paths obtained from Nakajima tests. The graph displays the relationship between major and minor stresses, indicating the material's response under various stress conditions. This analysis is essential for understanding the stress limits within which the material can be safely formed without failure. The hardening models, Swift and Voce, were used to predict forming limit stresses under different loading conditions: uniaxial, plane strain, and biaxial. The Swift and Voce hardening models set the limits for the material's FLSCs. The results suggest that the Swift model generally predicted higher forming limit stresses than the Voce model, especially under plane strain and biaxial conditions, which aligns with earlier observations by the strain-based forming limits. This verification demonstrates the accuracy of these models in predicting the forming limit stresses for DP590 grade high-strength steel, providing valuable insights into the material's behavior under multi-axial loading and its potential for formability in industrial applications.

The experimental and numerical results under uniaxial, plane strain, and biaxial loading conditions, as illustrated in Figure 10, highlight the impact of the selected hardening law on the predicted drawing depths. Finite element (FE) simulations based on the Hill'48 yield criterion, in conjunction with the Swift and Voce hardening models, were systematically validated against experimental measurements [13,16,17]. Under the uniaxial condition, the Swift and Voce models predicted drawing depths of 32.71 mm and 31.91 mm, respectively, compared to the experimental depth of 32.78 mm, corresponding to relative deviations of −0.21% and −2.65%. Under plane strain loading, the predicted values were 29.26 mm (Swift) and 28.94 mm (Voce), while the experimental measurement was 30. 23 mm, resulting in relative errors of −3.21% and −4.27%, respectively. Under the biaxial condition, the Swift model predicted 39.96 mm, while the Voce model predicted 39.78 mm, compared to the experimental value of 40.98 mm, yielding associated errors of −2.49% and −2.93%, respectively. These findings demonstrate that the Swift model provides superior predictive capability, exhibiting smaller deviations from experimental data across all deformation modes, particularly under complex biaxial loading conditions [31]. The analysis emphasizes the critical role of hardening law selection in accurately modeling the forming behavior and fracture mechanisms of high-strength steel sheets. Incorporating an appropriate hardening representation is therefore essential for improving the predictive accuracy and reliability of FE-based forming simulations involving multi-axial stress states.

It should be emphasized that three independent sets of tensile and Nakajima experiments were performed to validate the repeatability of the forming limit measurements. Across these repetitions, the comparative behavior of the Swift and Voce hardening laws was consistently reproduced, confirming that the observed differences are systematic rather than experimental artifacts. Although the present study was limited to a single sheet thickness, the availability of multiple comparative datasets strengthens the reliability of the conclusion that the Swift hardening law provides superior predictive accuracy, particularly under plane strain and biaxial loading paths. This consistency across experiments enhances confidence in the general applicability of the proposed framework for modeling the forming behavior of high-strength steels.

Although the present study focused exclusively on DP590 steel with a thickness of 1 mm, this limitation reflects the availability of materials and the defined scope of the experimental program. Nevertheless, the integrated framework developed here, combining the experimental forming limit characterization with FE simulations based on the Hill'48 yield criterion and two representative hardening laws remain broadly applicable to other advanced high-strength steel grades and thicknesses. Future research will extend this methodology to additional grades (e.g., DP780, DP980) and multiple thicknesses to enhance its generality and establish a more comprehensive database for industrial forming simulations.

To further highlight the novelty of this study, it is important to differentiate the present findings from previous works. Earlier

investigations on AHSS, particularly DP780 and DP980, have primarily focused on strain-based forming limit curves or employed a single hardening law in finite element simulations [19,22,24]. While these studies established useful forming limits, they did not systematically integrate strain- and stress-based approaches nor assess the predictive capability of multiple hardening models. In contrast, the present study integrates experimental FLCs and FLSCs of DP590 with FE simulations based on the Hill'48 yield criterion, incorporating both Swift and Voce hardening laws. This comprehensive framework enables simultaneous validation of forming limits under different loading paths and quantitative assessment of drawing depth predictions. Such comparisons have rarely been reported for the DP590 grade, making the present work distinct in scope and directly relevant to industrial applications, particularly in the automotive sector, where thin-gauge AHSS is increasingly utilized.

The industrial significance of this work lies in its direct applicability to real forming operations. Automotive stamping processes frequently involve multiaxial loading conditions and nonlinear strain paths, where the choice of hardening law has a critical influence on the accuracy of forming limit predictions. The demonstrated superiority of the Swift hardening model in reproducing experimental observations provides practical guidance for engineers seeking to improve simulation fidelity. Consequently, the proposed framework can support the design and optimization of forming processes for DP590 components, such as door reinforcements, cross-members, and crash-relevant structural parts, where accurate prediction of failure risk is essential for ensuring both safety and manufacturing efficiency.

6. Conclusions

This research employed both experimental and numerical approaches to investigate the forming behavior of high-strength steel sheets grade DP590. The FLCs and FLSCs were determined using the Nakajima and uniaxial tensile tests and subsequently validated through FE simulations based on the Hill'48 yield criterion with two hardening Swift and Voce models.

In the experimental phase, uniaxial tensile and Nakajima tests were conducted to capture the material's response under various strain paths, providing valuable information on the formability and fracture behavior of the steel sheets.

In the numerical phase, FE simulations were performed to predict FLCs and FLSCs, accounting for anisotropy and strain hardening to replicate real deformation behavior. The simulation results closely matched the experimental data, confirming the reliability of the computational models.

The Swift hardening model consistently predicted higher forming limit stresses and more accurate drawing depths than the Voce model, particularly under biaxial and plane strain conditions, demonstrating its suitability for simulating complex forming processes.

Although this study was limited to DP590 steel grade with the thickness of 1 mm, the integrated methodology is transferable to other high-strength steels and thicknesses. Future work will extend the framework to additional grades (e.g., DP780, DP980) and different thicknesses to enhance its generality and establish a broader database for industrial applications.

It should be noted that the mechanical property parameters derived in this study are strictly representative of the 1 mm thickness. While uniaxial tensile and Nakajima tests provided sufficient data for calibrating constitutive models and validating forming limits of the investigated sheet, the transferability of these parameters to other thicknesses of DP590 cannot be assumed. Thickness variations often influence microstructural constraints, strain hardening behavior, and fracture mechanisms. Therefore, the present results should be regarded as a reliable benchmark for the 1 mm sheet, while the proposed integrated framework can be readily extended to other thicknesses in future work to establish a more comprehensive material database.

It should be noted that fracture was not modeled using GTN-type criteria in this work. Instead, forming limits were determined based on localized necking observed in the Nakajima tests, with FE simulations serving to validate these experimentally derived limits.

By integrating experimental and numerical methods, this study provides a comprehensive and reliable framework for evaluating the formability of high-strength steels. The proposed methodology enhances the predictive accuracy of FE simulations and supports material selection and process optimization in the automotive and aerospace industries. Moreover, it can be extended to other material systems and forming conditions, making it a valuable tool for engineers and researchers involved in formability assessment and virtual process design.

Acknowledgments

This work was supported by the Office of the Permanent Secretary, Ministry of Higher Education, Science, Research and Innovation (OPS MHESI), and Thailand Science Research and Innovation (TSRI) under Grant No. RGNS 65–101, with additional support from Rajamangala University of Technology Isan (RMUTI) under Contract No. FF66-P5-006. The authors also thank Rajamangala University of Technology Isan, Sakon Nakhon Campus, and Thai Summit Automotive Co., Ltd. for their support.

References

[1] T. K. Roy, B. Bhattacharya, C. Ghosh, and S. K. Ajmani, "Advanced high strength steel: processing and applications," 1st ed, Springer Nature Singapore, 2018, 216 pages.

[2] F. A. Pérez-González, J. H. Ramírez-Ramírez, L. E. Hernández, M. A. Quiñones, N. F. Garza-Montes-de-Oca, and R. Colás, "Characteristics of advanced high-strength steels obtained by the compact strip production route," *Materials Science and Technology*, vol. 39, no. 3, pp. 327-337, 2023.

[3] S. Panich, M. Liewald, and V. Uthaisangsuk, "Stress and strain based fracture forming limit curves for advanced high strength steel sheet," *International Journal of Material Forming*, vol. 11, pp. 643-366, 2018.

[4] A. Nakwattanaset, S. Suranuntchai, and S. Panich, "Strain-and stress-based forming limit curves of DP440 steel sheet with application to the cross-die forming test," *AIP Conference Proceedings*, vol. 2279, p. 050004, 2020.

[5] T. Sirinakorn, S. Sodjit, and V. Uthaisangsuk, "Influences of microstructure characteristics on forming limit behavior of dual phase steels," *Steel Research International*, vol. 86, no. 11, pp. 1594-1609, 2015.

[6] L. Huang, and M. Shi, "Forming limit curves of advanced high strength steels: Experimental determination and empirical prediction," *SAE International Journal of Materials and Manufacturing*, vol. 11, no. 4, pp. 409-418, 2018.

[7] R. M. De A. Bornancin, C. P. Nikhare, and P. V. P. Marcondes, "Numerical comparison of advanced high strength steels forming limit curve using banabic and nakazima tests," International Journal on Interactive Design and Manufacturing, vol. 18, pp. 6469-6478, 2024.

[8] S. Panich, F. Barlat, V. Uthaisangsuk, S. Suranuntchai, and S. Jirathearanat, "Experimental and theoretical formability analysis using strain and stress based forming limit diagram for advanced high strength steels," *Materials and Design*, vol. 51, pp. 756-766, 2013.

[9] S. Kingklang, W. Julsri, T. Chiyatan, and V. Uthaisangsuk, "A comparative study of forming and crash behavior of high strength steels," *Materials Performance and Characterization*, vol. 8, no. 1, pp. 355-379, 2019.

[10] J. He, D. Zeng, X. Zhu, Z. C. Xia, and S. Li, "Effect of nonlinear strain paths on forming limits under isotropic and anisotropic hardening," *International Journal of Solids and Structures*, vol. 51, pp. 402-415, 2014.

[11] P. Rui, N. Peixinho, and S. L. Costa, "A review of sheet metal forming evaluation of advanced high-strength steels (AHSS)," *Metals*, vol. 14, no. 4, p. 394, 2024.

[12] Z. Marciniak, and K. Kuczyński, "Limit strains in the processes of stretch-forming sheet metal," *International Journal of Mechanical Sciences*, vol. 9, no. 9, pp. 609-612, 1967.

[13] R. J. Hill, "Constitutive modelling of orthotropic plasticity in sheet metals," *Journal of the Mechanics and Physics of Solids*, vol. 38, no. 3, pp. 405-417, 1990.

[14] F. Barlat, and L. Jianshe, "Plastic behavior and stretchability of sheet metals. part I: A yield function for orthotropic sheets under plane stress conditions," *International Journal of Plasticity*, vol. 5, pp. 51-66, 1989.

[15] F. Barlat, J. C. Brem, J. W. Yoon, K. Chung, R. E. Dick, D. J. Lege, F. Pourboghrat, S. Choi, and E. W. Chu, "Plane stress yield function for aluminum alloy sheets-part 1: Theory," *International Journal of Plasticity*, vol. 19, pp. 1297-1319, 2003.

[16] H. W. Swift, "Plastic instability under plane stress," *Journal of the mechanics and physics of solids*, vol. 1, no. 1, pp. 1-18, 1952.

[17] E. Voce, "The relationship between stress and strain for homogeneous deformations," *Journal of the Institute of Metals*, vol. 74, pp. 537-562, 1948.

[18] B. Liu, K. Zhang, F. Xiao, and J. Yang, "Application of constitutive model for high-strength steels in automobile: A review," *Steel Research International*, vol. 96, no. 11, pp. 30-64, 2025.

[19] S. Panich, K. Chongbunwatana, and T. Jantarasricha, "Formability evaluation of sheet metal forming on advanced high-strength steel via an integrative experimental-theoretical approach based on localized necking and fracture limits," *Journal of Mechanical Science and Technology*, vol. 5, pp. 5389-5404, 2021.

[20] G. J. Béres, Z. Weltsch, R. Borbély, M. L. Kölüs, Z. Lukács, and M. Tisza, "An extended stress-based forming limit diagram focusing on the wrinkling phenomenon and the effect of the normal pressure on clamped surfaces," *Journal of Materials Processing Technology*, vol. 322, p. 118196, 2023.

[21] M. Zhang, Z-q. Cheng, Y-k Chen,Y. Wang, Z-p. Zou, Z-l. Mi, and Y. Li, "A novel dual-stage failure criterion based on forming limit curve for uncured glare," *Journal of Materials Processing Technology*, vol. 332, p. 118567, 2024.

[22] F. Shen, Y. Sparrer, J. Rao, M. Könemann, S. Münstermann, and J. Lian, "A forming limit framework accounting for various failure mechanisms: Localization, ductile and cleavage fracture," *International Journal of Plasticity*, vol. 175, p. 103921, 2024.

[23] T. Huang, M. Zhan, K.Wang, F. Chen, J. Guo, Y. Li, Z. Song, and L. Bai, "Forming limit stress diagram prediction of pure titanium sheet based on GTN model," *Materials*, vol. 12, no. 11, p. 1783, 2019.

[24] H. Cui, L. Di, F. Qiutao, L. Zipeng, X. Jiachuan, and J. Ning, "Research on forming limit stress diagram of advanced high strength dual-phase steel sheets," *Materials*, vol. 16, no. 13, p. 4543, 2023.

[25] T. B. Stoughton, "A general forming limit criterion for sheet metal forming," *International Journal of Mechanical Sciences*, vol. 42, pp. 1-17, 2000.

[26] Z. Zhu, and I. L. Al-Qadi, "Crack detection of asphalt concrete using combined fracture mechanics and digital image correlation," *Journal of Transportation Engineering*, *Part B: Pavements*, vol. 149, no. 3, p. 04023012, 2023.

[27] N. Amraish, A. Reisinger, and D. Pahr, "A novel specimen shape for measurement of linear strain fields by means of digital image correlation," *Scientific Reports*, vol. 11, p. 17515, 2021.

[28] R. Hill, "A theory of the yielding and plastic flow of anisotropic metals, proceedings of the royal society of london. series A," *Mathematical and Physical Sciences*, vol. 193, pp. 281-297, 1948.

[29] T-T. Luyen, T-B. Mac, and D-T. Nguyen, "Simulation and experimental comparison study based on predicting forming limit curve of SUS304 sheet material," *Modern Physics Letters B*, vol. 37, no. 16, p. 2340001, 2023.

[30] C. Bonatti, and D. Mohr, "Neural network model predicting forming limits for bi-linear strain paths," *International Journal of Plasticity*, vol. 137, p. 102886, 2021.

[31] S. Zhang, S. Zhang, H. Ye, L. Zhou, N. Yuan, and C. Zhou, "Hardening behavior and prediction of ductile fracture during AA7075-T651 sheet metal forming," *Journal of Materials Engineering and Performance*, vol. 32, pp. 10455-10468, 2023.